Nuclear Engineering and Technology xxx (xxxx) xxx

Contents lists available at ScienceDirect

Nuclear Engineering and Technology

journal homepage: www.elsevier.com/locate/net

Original Article

An improved two-temperature method for computing the temperature distributions within a TRISO-coated particle pebble fuel

Dali Yu [a,*], Fangnian Wang [b], Huaping Mei [a], Xiongwei Cheng [a], Chengjun Duan [a]

[a] Institute of Nuclear Energy Safety Technology (INEST), Hefei Institutes of Physical Science, Chinese Academy of Sciences, Shushanhu Road 350, Hefei, 230031, China

[b] Institute of Thermal Energy Technology and Safety (ITES), Karlsruhe Institute of Technology (KIT), Kaiserstraße 12, Karlsruhe, 76131, Germany

ARTICLE INFO

Keywords:
Two-temperature method
Coated particle fuel
Pebble fuel
TRISO
Finite element method

ABSTRACT

With the world's first pebble-bed modular high-temperature gas-cooled reactor beginning commercial operation in China, the tristructural-isotropic (TRISO) coated particle pebble fuel technology has garnered significant research interest and widespread attention. In light of the fact that temperature gradients within a pebble fuel may span several hundred degrees Celsius, it becomes imperative to attain a more precise and rapid determination of the internal temperature distribution. This work first developed an Improved Two-temperature Method (ITM) based on the analogous nature of heat and neutron diffusion processes, with deriving equations for three parameters k_f, k_m, and μ, to achieve higher accuracy and wider application range. Then, seven tests were implemented for validating the ITM through comparing with finite element method, which can be considered identical with the analytic solution. Results show that the ITM can provide very accurate predictions of the peak temperature of both the fuel particles and the matrix. Finally, analysis of the influences of packing fraction and particle diameter on the temperature distribution within a pebble fuel, has been investigated, and it was found that there are two competing mechanisms resulting in the optimized design occurs at the packing fraction of 0.05, and the smallest particle diameter of 0.2 mm. The developed ITM and findings in this work provide tools and thermal conditions for analyzing fission gas release, creep rate, and other performance metrics of the pebble fuel.

1. Introduction

The Tristructural-Isotropic (TRISO) coated particle pebble fuel, known for its exceptional high-temperature resilience and sustained performance during high burnup, has garnered significant research interest [1]. Initially integrated into the AVR (Arbeitsgemeinschaft Versuchsreaktor) pebble-bed reactor in Germany, the application of TRISO fuel expanded to the South African Pebble Bed Modular Reactor [2]. Presently, TRISO fuel is a key technique in China's 250 MW_t High-Temperature Gas-Cooled Reactor within the national nuclear power demonstration project [1]. Recognized for its innovation, TRISO coated particle fuel technology is considered highly compatible with High-Temperature Gas-Cooled Reactors and has been selected as a prospective design for the fourth-generation Very High-Temperature Reactor (VHTR) under the Next Generation Nuclear Plant (NGNP) project [3]. Research initiatives have also explored the potential for TRISO-like fuels in diverse nuclear reactors, including Light Water Reactors [4,5], Molten Salt Reactors [6], S-CO_2 Cooled Reactors [7–9], novel Heat Pipe Reactors [10–12], and other Special Purpose High Temperature Reactors [13,14].

A typical TRISO-coated particle pebble fuel consists of a fueled region and a surrounding thin non-fueled graphite shell. The fueled region has a radius of approximately 25 mm, including a graphite matrix and $10,000 \sim 15,000$ dispersed TRISO particles [15], as shown in Fig. 1. A TRISO particle consists of five distinct regions. At its nucleus lies the fuel kernel, commonly anoxide, carbide, or an oxycarbide formulation that harbors the fissile material. A porous carbon buffer encircles the kernel, mitigating the kinetic energy of recoiling fission fragments and accommodating the particle's dimensional irregularities along with the containment of internally generated gases. The outer layers consist of an inner pyrolytic carbon (IPyC) layer, a silicon carbide (SiC) layer, and an outer pyrolytic carbon (OPyC) layer. These complexities of geometry pose substantial challenges to accurately calculating the thermal behavior of TRISO fuels [16].

Paul Van Uffelen emphasized the challenges in advanced fuel development, and highlighted the need for precise predictions of fuel rod performance to ensure safety and cost-effectiveness, with a particular

* Corresponding author.
E-mail address: dlyu@inest.cas.cn (D. Yu).

https://doi.org/10.1016/j.net.2025.103515
Received 21 November 2024; Received in revised form 25 December 2024; Accepted 26 January 2025
Available online 4 February 2025

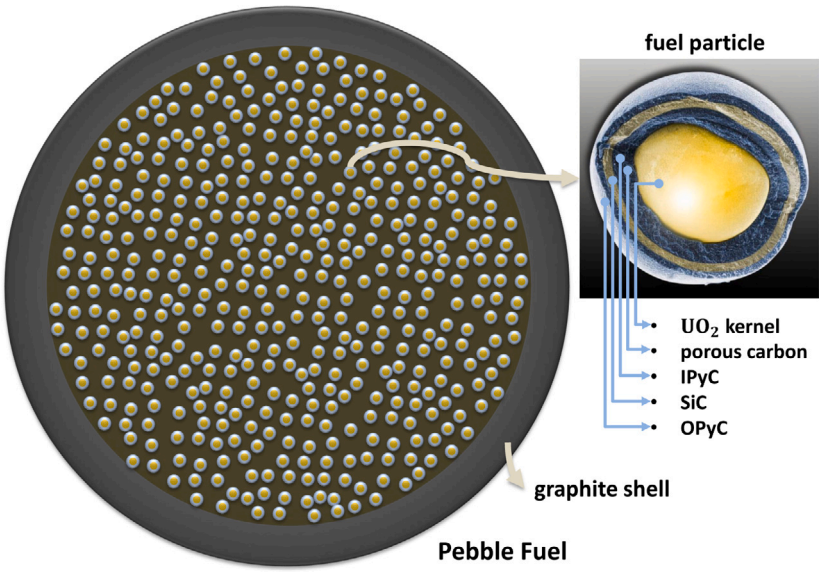

Fig. 1. Schematic diagram of a TRISO-coated particle pebble fuel.

emphasis on accurate heat transfer modeling [17]. Standard modeling practice currently simplifies the pebble fuel structure to an isotropic, two-component, heterogeneous, macro-scale porous medium [18–20]. Generically, the averaging volume method is adopted for the homogenization treatment of the pebble fuel [21–23]. The volumetric-average approach is non-conservative and would underestimate the fuel temperature, while the harmonic-average approach overvalues the effect of the low thermal conductivity of fuel particles that would derive a much lower average thermal conductivity. The center temperature of the pebble fuel predicted by these two conductivities can deviate by several hundred degrees Celsius. Therefore, These two average thermal conductivities serve as upper and lower bounds respectively, referred as Wiener bounds [24]. The Wiener bounds were used to provide comparisons with the developed two-temperature method in this work. Numerous models have been proposed to predict effective thermal conductivities of the fuel elements, among which, the Chiew and Glandt model [25] and the Maxwell model [26] are considered as the most well-known models. Meanwhile, Liu proposed a two-regime heat conduction model grounded in the assumption of centrally dense packing of fuel particles within the fuel [27,28]. The model serves as an effective tool for predicting maximum and mean temperatures in nuclear fuels with heat-emitting particles. In comparison to existing models, Liu's offers conservative temperature estimates and demonstrates enhanced concordance with both peak and average fuel temperatures of the simulated compacts and pebbles. Cai implemented thermo-mechanical simulations of TRISO particle embedded plate fuel, integrating multi-physical effects such as plastic deformation, irradiation swelling, creep, and gap heat transfer [29]. Nonetheless, thermal conductivity within these simulations was determined using empirical correlations, which resulted in reduced simulation accuracy and limited application arrange. Wang developed three multi-scale heat conduction models including the Multi-region Layered model, Multi-region Non-layered model, and Homogeneous model for fully ceramic micro-encapsulated fuel pellet, the whole fuel pellet was taken as the homogeneous material in the Homogeneous model [30,31]. Jiang provides a detailed description of the models used by BISON code for TRISO fuel [32], along with a set of problems that test these models by comparing them both with another code and experimental data. Empirical correlations underpin the modeling of the fuel's thermal conductivity for rigorous quantification of heat transfer phenomena. Gong employs the finite element method to simulate the effective thermal conductivity of three-dimensional, fully ceramic microencapsulated fuel pellets [33]. Wang improved and refined a three-dimensional fuel pebble heat transfer and Monte Carlo neutron coupled model. The model incorporates a random distribution of TRISO fuel particles and a precise geometric model, in which the heat conduction calculation is performed using an existing effective thermal conductivity correlation [34,35]. The conducted finite element analysis reveals that there is an inverse correlation between the effective thermal conductivity of the pellet and the volume fraction of TRISO particles. Moreover, the spatial distribution of these particles notably influences the pellet's effective thermal conductivity. Although this finite element method yields precise temperature calculations, it is computationally intensive.

In light of the fact that temperature gradients within a pebble fuel may span several hundred degrees Celsius, it becomes imperative to attain a more precise and rapid determination of the internal temperature distribution, which is the thermal condition for analyzing fission gas release, creep rate, and other performance metrics in evaluating the so called "walk-away" safety features of the High Temperature Gas-cooled Reactor (HTGR). Consequently, it is essential to regard the fuel particles and graphite matrix discretely in the analytical framework. Shentu developed a Monte Carlo method for heat conduction analysis in intricate geometries [36], drawing upon theoretical insights from asymptotic analyses of the neutron transport equation. This method capitalizes on the analogous nature of heat and neutron diffusion processes, both of which are typified by non-absorptive behavior, a stationary source, and a uniform velocity scenario. To seek the deterministic techniques for determining the realistic temperature distribution, a two-temperature homogenized model was proposed [37]. However, the model does not consider the high temperature gradation in a pebble due to the homogenized conductivity is used. What is more, the two-temperature homogenized model uses three parameters k_f, k_m, μ that determined by an optimization process relates to the Monte Carlo method calculation results, they are inconvenient to be obtained in the actual application, this motivates our work in improving the two-temperature method mainly by proposing new equations for three parameters k_f, k_m, and μ.

Therefore, building upon the foundation of previous work [37], the authors proposed an improved two-temperature method (ITM) based on the analogous nature of heat and neutron diffusion processes, with deriving new equations for three parameters k_f, k_m, and μ, to achieve higher accuracy, wider application range, and extending application for transient process. This paper would briefly describe the modeling of ITM in Section 2 and numerical approach in Section 3, and the ITM validation is introduced in Section 4, then analyze the influences of packing fraction and particle diameter in Section 5, while main points are concluded in Section 6.

2. Improved Two-temperature Method (ITM)

ITM capitalizes on the analogous nature of heat and neutron diffusion processes, both of which are based on the fundamental governing differential equation that the increasing heat in the control region equals the sum of the heat across all the surfaces of the region and the heat transferred from the region to the adjacent other material. ITM is not only convenient to perform but also gives more realistic results since particles and graphite matrix are considered separately.

2.1. Main equations

When applies the ITM in determining the temperature distributions within a TRISO-coated particle pebble fuel, the following constrains are made,

- There are only two components, fuel particles and graphite matrix.
- Graphite matrix is continuous everywhere.
- No particles contact with each other, means particles could never form continuous conduction pathways.
- The temperature is uniform across the outer surface of the pebble fuel.

ITM can be applied to many different geometric structures. When used for the TRISO-coated particle pebble fuel with spherical structure, the equations of the ITM is written in the following form:
fueled zone:

$$\begin{aligned} A_f k_f \nabla^2 T_f(r,t) - \mu\left[T_f(r,t) - T_m(r,t)\right] + q(t) &= \varepsilon M_f \frac{\partial T_f(r,t)}{\partial t} \\ A_m k_m \nabla^2 T_m(r,t) + \mu\left[T_f(r,t) - T_m(r,t)\right] &= (1-\varepsilon) M_m \frac{\partial T_m(r,t)}{\partial t} \end{aligned} \tag{1}$$

non-fueled shell:

$$k_s \nabla^2 T_s(r,t) = M_s \frac{\partial T_s(r,t)}{\partial t}$$

where, k_f is the thermal conductivity of fuel particle, k_m is the thermal conductivity of graphite matrix in the fueled zone, k_s is the thermal conductivity of graphite shell. T_f is the temperature at the center of fuel particle, T_m is the temperature of graphite matrix, T_s is the temperature of graphite shell. A_f is the ratio of fuel particle diffusion surface area to the complete surface area, A_m is the ratio of graphite matrix diffusion surface area to the complete surface area. μ is the region heat transfer coefficient. q is homogenized volumetric heat generation rate. M_f, M_m, M_s are volumetric heat capacities of fuel particle, graphite matrix, and graphite shell, respectively. The volumetric heat capacity M herein is defined as the product of specific heat capacity and mass density. ε is the actual packing fraction of the particles.

As Eqs. (1) describes, the heat transfer process in a pebble fuel is analogous to the two-group neutron diffusion process characterized by no absorption, no fission, and a fixed source. T_f is regarded as the fast neutron flux and T_m is the thermal neutron flux. Heat transfer between the two groups is assumed only to execute in the direction from higher temperature region to the lower region, and this is similar to the principle in the transfer between the fast neutrons and the thermal neutrons. Accounting for the region heat transfer term is driven by the temperature difference, the heat transferred from local region to the adjacent other material can be calculated by the relationship, $\mu\left[T_f(r,t) - T_m(r,t)\right]$. The diffusion term expresses the heat migrating across all surfaces of the region. The fueled zone is divided into two regions, the graphite matrix region and the fuel particles region. Heat transfer is not entirely along the full radial direction in these two regions, therefore coefficients A_f and A_m are needed to represent the proportion of heat transport for these two parts, with the sum of these two coefficients being 1, representing the total heat diffusion surface area in the radial direction.

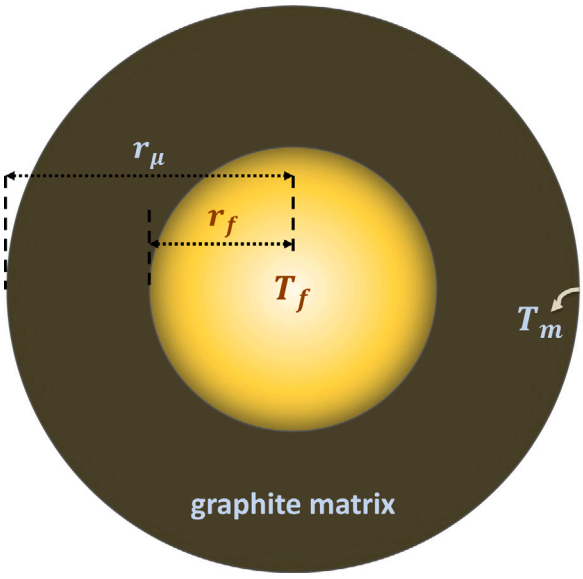

Fig. 2. Calculation model for parameter μ.

2.2. Determination of μ, A_f, A_m

In Eqs. (1), a TRISO particle is treated as an object, surrounded by spherical and continuous graphite matrix, as shown in Fig. 2. T_f is the temperature at the center of fuel particle, T_m is the temperature of graphite matrix, which is the temperature of graphite matrix outer boundary in the calculation model for parameter μ. Therefore, the region heat transfer term $\mu\left[T_f(r,t) - T_m(r,t)\right]$ indicates the heat transferred from the fuel particle to the adjacent graphite matrix while the temperature at the center of the fuel particle is T_f and the boundary temperature of the matrix is T_m. To determine the coefficient μ, the region heat transfer term can be treated to calculate the volumetric heat generation rate in the total region.

Assuming the heating power of the single fuel particle used to maintain such thermal conditions as shown in Fig. 2, is Q_μ. Then, the following equation can be derived:

$$\mu\left[T_f(r,t) - T_m(r,t)\right] = \frac{Q_\mu(t)}{V_\mu} \tag{2}$$

where, V_μ is the volume of the hypothetical calculation model for parameter μ.

Heat transported in the fuel particle and the graphite matrix can be described as below:

$$\begin{aligned} \int_0^{r_f} \frac{r}{3}\frac{Q_\mu(t)}{V_f}\mathrm{d}r &= \int_0^{r_f} -k_f \frac{\partial T(r,t)}{\partial r}\mathrm{d}r \\ \int_{r_f}^{r_\mu} \frac{Q_\mu(t)}{4\pi r^2}\mathrm{d}r &= \int_{r_f}^{r_\mu} -k_m \frac{\partial T(r,t)}{\partial r}\mathrm{d}r \end{aligned} \tag{3}$$

where, r_f and r_μ are the radius of the fuel particle and the whole calculation model respectively, as shown in Fig. 2. This equation can be transformed into the following form:

$$\frac{1}{\mu} = \frac{r_\mu^3}{6k_f r_f} + \frac{r_\mu^3 - r_\mu^2 r_f}{3k_m r_f} \tag{4}$$

The variable V_μ indicates the volume that a single fuel particle occupies in a fuel pebble. Assuming the volume of the fuel pebble is V_p, then the following equation can be defined:

$$V_\mu = \frac{FV_p}{n};\ r_\mu = \left(\frac{3V_\mu}{4\pi}\right)^{1/3} \tag{5}$$

where, F is an empirical coefficient relevant to the packing fraction of particles, n is the number of fuel particles in a fuel pebble.

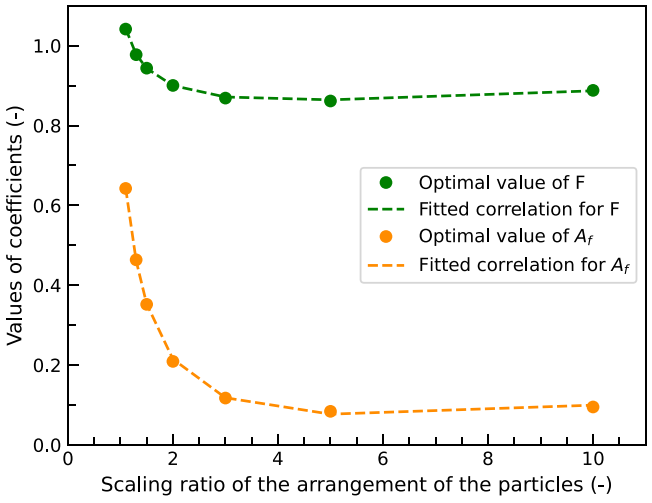

Fig. 3. Curve fitting for coefficients F, A_f, A_m.

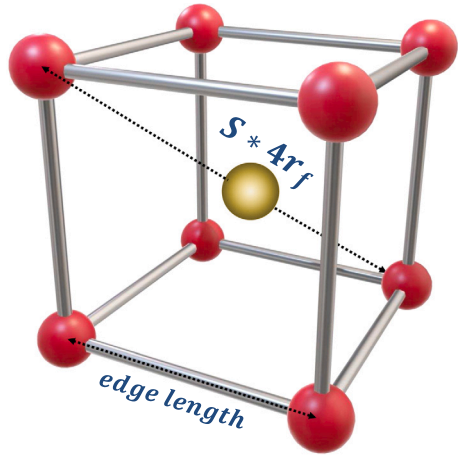

Fig. 4. Calculation model for scaling ratio S in BCC arrangement.

In this work, the coefficients F, A_f, A_m were proposed and best estimated. Seven cases with different scaling ratios of the arrangement of the particles, ranging from 1.1 to 10, were used. Details of the cases are introduced in Table 1. As Fig. 3 shows, by exploring the values of F and A_f, making the root mean square error of the particles and matrix temperature values predicted by ITM minimized comparing with results of the finite element method, which would be introduced in the paper, then the optimal values are obtained. By analyzing the influences of parameters on these optimal values, the coefficients F, A_f, and A_m were found only relate to the scaling ratio of the arrangement of the particles. Herein, the correlations are eventually fitted through Python scipy library and given as below:

$$\begin{aligned} F &= \left(\frac{S+3.12}{\ln(S)+0.2}\right)^{0.12} - 0.333 \\ A_f &= \frac{S+1}{[\ln(S)+1.255]^{2.55}} - 0.333 \\ A_m &= 1 - A_f \end{aligned} \tag{6}$$

where, S is the scaling ratio of the arrangement of the particles.

As Fig. 4 shows, the particles are distributed in Body-Centered Cubic (BCC) structure. Then the scaling ratio S can be correlated with the packing fraction ε of a standard module, the equation is derived as below:

$$S = \left(\frac{\sqrt{3}\pi}{8\varepsilon}\right)^{1/3} \tag{7}$$

In the conventional pebble fuel modeling process, the packing fraction ε can be obtained as the input parameter, and the scaling ratio can be obtained by Eqs. (7), then the parameters A_f and A_m can be obtained by substituting Eqs. (6), and finally the coefficient μ can be obtained by Eqs. (5) and (3).

2.3. Computing flow diagram of ITM

As Fig. 5 shows, the computing procedure begins at preparing "Inputs", e.g. number of TRISO particles, geometries of TRISO particles, geometries of fuel pebble, thermal properties of all materials, other thermal conditions and simulations related parameters. After completes the inputs, the key parameters μ, A_f, A_m can be calculated. Then, starts the temperature distribution calculation for the first step, until the total simulation time is reached.

3. Numerical approach for comparisons

Though a typical TRISO-coated particle pebble fuel contains 10,000~15,000 dispersed TRISO particles, these complexities of geometry can be modeled using finite element method with high-performance computing technique, the results should be identical with the analytic solution. In this work, ANSYS CFX software would be used to calculate the heat transport in a pebble fuel, providing results for validation of the developed ITM. Meanwhile, the Wiener bounds [24], introduced in Section 1, are used to provide comparisons with ITM in the analysis of internal heat transfer in a pebble fuel.

3.1. Finite element method

In order to reduce unnecessary modeling work, the fuel pebble model is simplified as numerous UO_2 particles uniformly dispersed in a graphite matrix without graphite shell when using this finite element method to validate the ITM. Fig. 6 shows the modeling process of finite element method. First, Python is used to calculate the position of each TRISO fuel particle within a pebble fuel as well as the size of the pebble fuel, with the number of particles simulated fixed at 1411. Density boxes are generated around each particle for the purpose of mesh refinement. All the information is compiled into an RPL script file that is readable by ANSYS ICEM through Python. Then, uses ANSYS ICEM to automatically generate unstructured mesh and optimize the mesh quality to better than 0.4. Finally, the thermal conditions of the pebble fuel are set in ANSYS CFX, and the high-precision steady-state equation is used to calculate, and the iterative error is less than 10^{-7}. The temperature distributions of the particles and matrix are extracted using CCL script in ANSYS CFD-Post.

Mesh independent study has been implemented for this finite element method. Seven cases for validating ITM were calculated and the number of mesh elements are around 30 million for each. For all cases, the particle diameter is 0.5 mm, particle numbers is 1411, and the arrangement applied for the particle distribution is BCC.

3.2. Wiener bounds

The volumetric-average approach is non-conservative and would underestimate the fuel particle temperature, while the harmonic-average approach overvalues the effect of the low thermal conductivity of fuel particles that would derive a much lower average thermal conductivity. These two average thermal conductivities serve as upper and lower bounds respectively, referred as Wiener bounds. In this work, the Wiener bounds are used for comparisons with ITM in both the

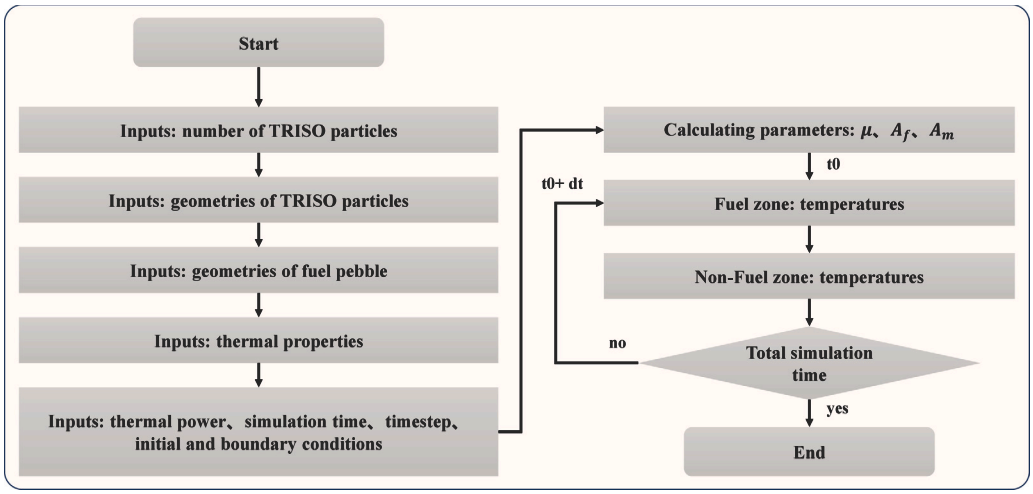

Fig. 5. Computing flow diagram of ITM.

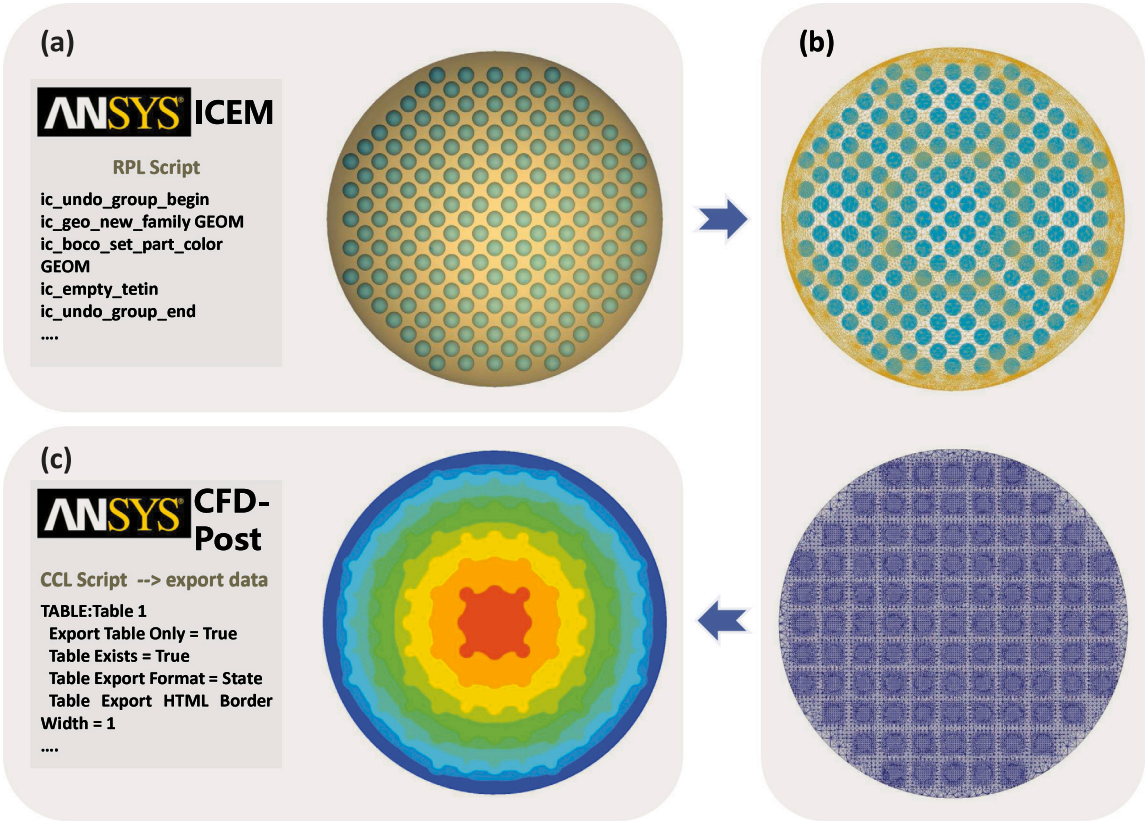

Fig. 6. Modeling process of finite element method: (a) generation of geometry and mesh density box; (b) unstructured mesh generation and optimization; (c) thermal calculations and results data extraction.

validation and analysis.

volumetric-average:

$$k_e = \left(V_f k_f + V_m k_m\right) / \left(V_f + V_m\right) \tag{8}$$

harmonic-average:

$$k_e = \left(V_f + V_m\right) / \left(V_f / k_f + V_m / k_m\right)$$

where, k_e is the predicted effective thermal conductivity of the pebble fuel. k_f is the thermal conductivity of fuel particle, k_m is the thermal conductivity of graphite matrix. V_f is the total volume of all fuel particles and V_m is the matrix occupied volume.

4. Results

As shown in Table 1, this study compares the results of the finite element method with those of the ITM across seven different tests. All conditions utilize the same particle number, particle diameter, and particle arrangement. The range of packing fractions covers almost all possible scenarios. Herein the packing fraction means the volumetric ratio of all particles to the pebble. The choice of boundary temperature and pebble thermal power does not affect the computational accuracy of the ITM. Meanwhile, for all the tests, the value of thermal conductivity k_f is 3 W/(mK), the value of thermal conductivity k_m is 20 W/(mK), the value of volumetric heat capacity M_f is 2 000 000 J/(m^3 K), the

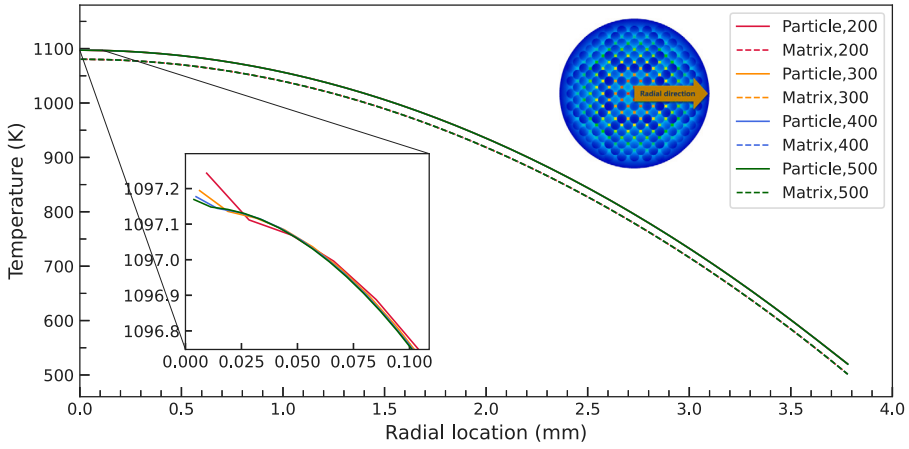

Fig. 7. Independence study of mesh elements on ITM.

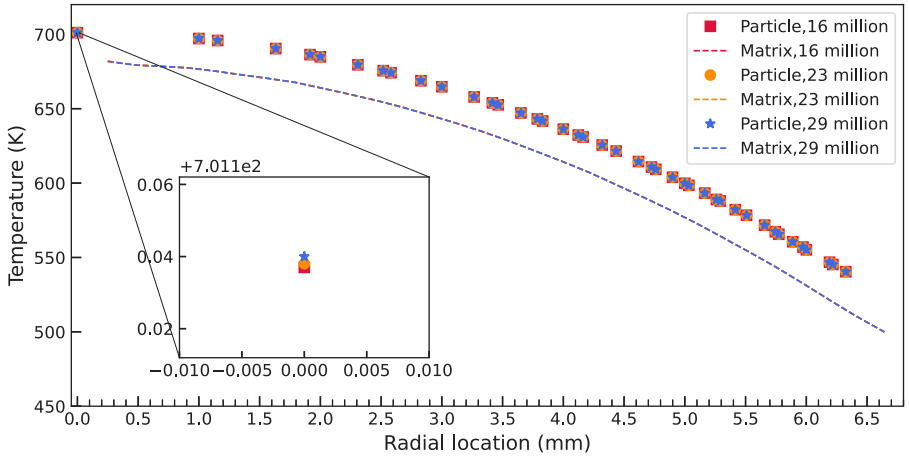

Fig. 8. Independence study of mesh elements on FEM.

Table 1
Information of the tests for validating ITM.

CASES	Scaling ratio S [–]	Particle numbers [–]	Particle diameter [mm]	Pebble diameter [mm]	Particle arrangement [–]	Packing fraction [–]	Pebble thermal power [W]	Boundary temperature [K]
CASE1	1.1	1411	0.5	7.569	BCC	0.407	500	500
CASE2	1.3	1411	0.5	8.839	BCC	0.255	500	500
CASE3	1.5	1411	0.5	10.110	BCC	0.171	500	500
CASE4	2.0	1411	0.5	13.285	BCC	0.0752	500	500
CASE5	3.0	1411	0.5	19.636	BCC	0.0233	500	500
CASE6	5.0	1411	0.5	32.338	BCC	0.00522	500	500
CASE7	10.0	1411	0.5	64.092	BCC	0.00067	500	500

value of volumetric heat capacity M_m is 1 800 000 J/(m^3 K). For all the tests, the key parameters μ, A_f, A_m are constants, only relates to the geometries and thermal properties, and the values are listed in Table 2.

4.1. Independence study

In order to reduce the impacts of mesh elements that used in both ITM and FEM, independence studies have been implemented on Case1 and Case4, respectively. ITM is one-dimensional in the radial direction programmed in this work. Four different numbers of radial mesh elements of 200, 300, 400, and 500 were used for the independence verification of the ITM. Three different numbers of mesh elements of 16 million, 23 million, and 29 million were used for the independence verification of the FEM. Herein, in order to reduce unnecessary modeling work, the fuel pebble model is simplified as numerous UO_2 particles uniformly dispersed in a graphite matrix without graphite shell in the simulations by both the ITM and the FEM.

Table 2
Information of key parameters of the tests for validating ITM.

CASES	Region heat transfer coefficient μ [W/(m^3 K)]	Ratio A_f [–]	Ratio A_m [–]
CASE1	103907405	0.64	0.36
CASE2	67 843 236	0.46	0.54
CASE3	46 115 130	0.35	0.65
CASE4	20 591 646	0.21	0.79
CASE5	6 361 175	0.12	0.88
CASE6	1 395 356	0.077	0.923
CASE7	170 922	0.0995	0.9005

Table 3
Thermal calculation results of FEM and ITM.

CASES	FEM		ITM	
	$T_{f,max}$ [K]	$T_{m,max}$ [K]	$T_{f,max}$ [K]	$T_{m,max}$ [K]
CASE1	1096.13	1076.93	1097.17	1077.96
CASE2	889.55	870.33	888.35	869.11
CASE3	799.36	780.13	799.71	780.50
CASE4	701.14	681.85	702.19	682.93
CASE5	631.90	612.45	632.04	612.52
CASE6	586.13	566.22	585.80	565.80
CASE7	554.65	533.73	554.75	533.87

Fig. 7 shows the steady-state temperature distributions of the particle and matrix in a pebble fuel. The temperature of the particle is the temperature at the center of the fuel kernel. The comparison results indicate that the maximum difference of the predicted temperature in the whole pebble fuel is less than 0.1 K when the number of radial mesh elements increases to 500. Therefore, 500 radial mesh elements is adopted in the ITM analysis of this work to ensure the computational accuracy.

Fig. 8 shows the FEM results of steady-state temperature distributions of the particle and matrix in a pebble fuel. The temperature of the particle is the temperature at the center of the fuel kernel. The comparison results indicate that the maximum difference of the predicted temperature in the whole pebble fuel is less than 0.01 K when the number of mesh elements increases to 29 million. Therefore, 29 million mesh elements is adopted in the FEM analysis of this work to ensure the computational accuracy.

4.2. Comparison with numerical approach

Seven tests were implemented for comparing ITM with FEM, including CASE1, CASE2, CASE3, CASE4, CASE5, CASE6, and CASE7. The condition details of all the tests are shown in Table 1, and the thermal calculation results of both the ITM and FEM are included in Table 3, which shows the predicting errors of all the cases are less than 1.2 K. As Fig. 9(a) shows, the scaling ratio of the particles arrangement S equals 1.1, the fuel particles are compactly spaced together, and the peak temperature occurs at the center of the pebble fuel. The temperature at the center of the fuel particle T_f is about 20 K higher than the matrix temperature T_m, and the temperature gradient of the entire pebble fuel is about 600 K. As Fig. 9(b) shows, the scaling ratio of the particles arrangement S equals 1.3, the fuel particles are closely spaced together, and the peak temperature occurs at the center of the pebble fuel. The temperature at the center of the fuel particle T_f is about 20 K higher than the matrix temperature T_m, and the temperature gradient of the entire pebble fuel is about 400 K. As Fig. 9(c) shows, the scaling ratio of the particles arrangement S equals 1.5, the fuel particles are normally spaced together, and the peak temperature occurs at the center of the pebble fuel. The temperature at the center of the fuel particle T_f is about 20 K higher than the matrix temperature T_m, and the temperature gradient of the entire pebble fuel is about 300 K. As Fig. 9(d) shows, the scaling ratio of the particles arrangement S equals 2.0, the fuel particles are normally spaced together, and the peak temperature occurs at the center of the pebble fuel. The temperature at the center of the fuel particle T_f is about 20 K higher than the matrix temperature T_m, and the temperature gradient of the entire pebble fuel is about 200 K. As Fig. 9(e) shows, the scaling ratio of the particles arrangement S equals 3.0, the fuel particles are normally spaced together, and the peak temperature occurs at the center of the pebble fuel. The temperature at the center of the fuel particle T_f is about 20 K higher than the matrix temperature T_m, and the temperature gradient of the entire pebble fuel is about 130 K. As Fig. 9(f) shows, the scaling ratio of the particles arrangement S equals 5.0, the fuel particles are sparsely arranged together, and the peak temperature occurs at the center of the pebble fuel. The temperature at the center of the fuel particle T_f is about 20 K higher than the matrix temperature T_m, and the temperature gradient of the entire pebble fuel is about 90 K. As Fig. 9(g) shows, the scaling ratio of the particles arrangement S equals 10.0, the fuel particles are sparsely arranged together, and the peak temperature occurs at the center of the pebble fuel. The temperature at the center of the fuel particle T_f is about 20 K higher than the matrix temperature T_m, and the temperature gradient of the entire pebble fuel is about 50 K.

4.3. Influences of packing fraction and particle diameter

ITM was used to investigate the influences of packing fraction and particle diameter on the temperature distribution within a pebble fuel. As Fig. 10 shows, the diameter of the pebble fuel is 20 mm, the particle diameter is 0.5 mm, the total heating power of the pebble fuel is 500 W, and 100 cases of packing fractions uniformly ranging from 0.003 to 0.66 were analyzed through ITM. As Fig. 11 shows, the diameter of the pebble fuel is 20 mm, the packing fraction is 0.4, the total heating power of the pebble fuel is 500 W, and 100 cases of particle diameters uniformly ranging from 0.2 mm to 2 mm were analyzed through ITM. When the particle diameter equals 2 mm, the peak particle temperature achieves the highest value, which is considered as the worst design.

5. Discussion

From the results as shown in Fig. 9, it can be seen that the ITM can provide very accurate predictions of the peak temperature of both the fuel particles and the matrix. The temperature distributions within the pebble fuel are also well predicted, though the ITM seems like to underestimates the particle temperature and overestimates the matrix temperature around the outer boundary region of the pebble fuel. The reason could be the boundary temperatures of both particle and matrix are not properly solved, since the packing fraction around the boundary region of the pebble fuel is varying a lot from the average, caused by the geometry shape and arrangement. When the scaling ratio of the particles arrangement S is less than 3.0, the Winer Bounds can provide temperature bounds for both the particle temperature and matrix temperature, however, the prediction errors of the Winer Bounds in all the cases are obvious.

As shown in Fig. 10, when the packing fraction ε equals 0.66, the peak particle temperature achieves the highest value, which is considered as the worst design. When the packing fraction ε equals 0.05, the peak particle temperature achieves the lowest value, which is considered as the optimized design. When the packing fraction ε decreases, the heating power of a single particle increases, which would lead higher peak particle temperature. Meanwhile, the volume

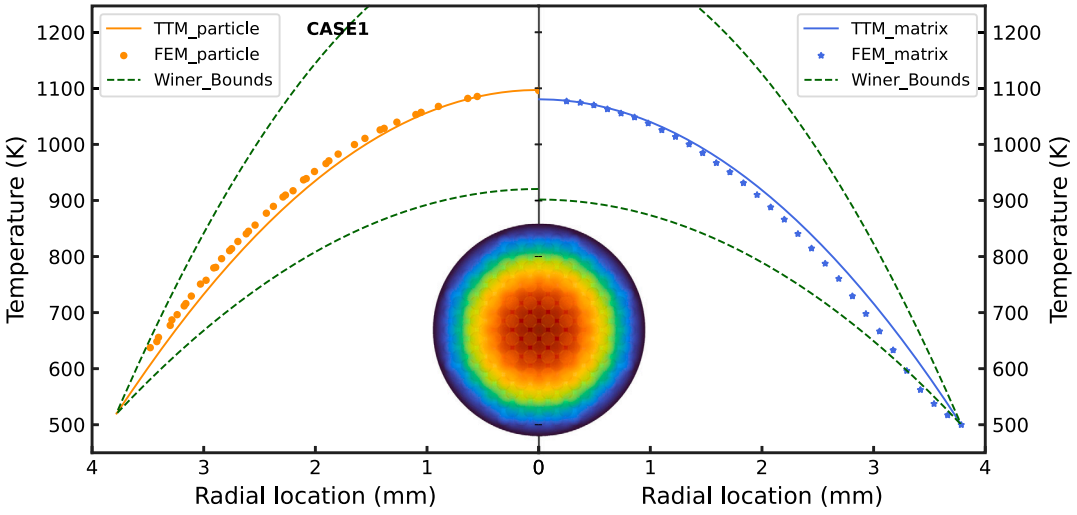

(a) CASE1, $S = 1.1$

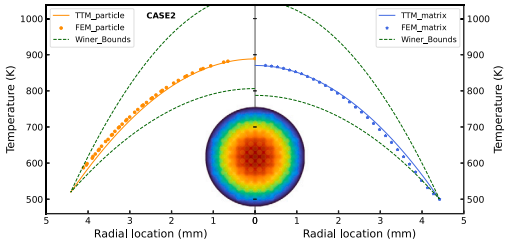

(b) CASE2, $S = 1.3$

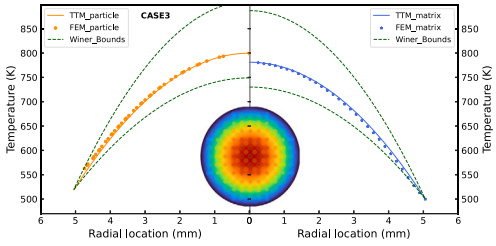

(c) CASE3, $S = 1.5$

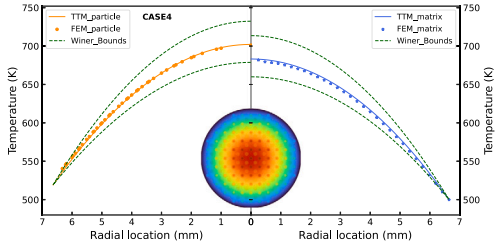

(d) CASE4, $S = 2.0$

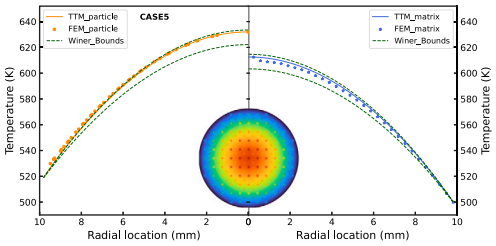

(e) CASE5, $S = 3.0$

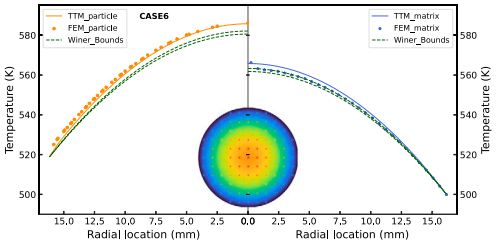

(f) CASE6, $S = 5.0$

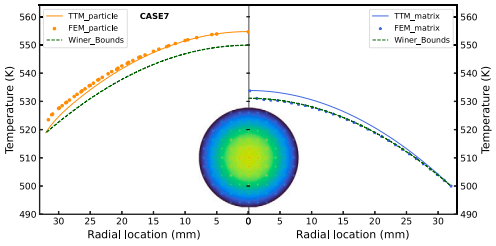

(g) CASE7, $S = 10.0$

Fig. 9. Comparisons of temperature distributions of particle and matrix in different tests.

fraction of the particle decreases, the average thermal conductivity of the pebble fuel would increase since the particle thermal conductivity is much lower than the matrix thermal conductivity, and this would lead lower particle temperature distribution within a pebble fuel. These two competing mechanisms result in the optimized design occurring at the packing fraction ε of 0.05.

As shown in Fig. 11, when the particle diameter equals 0.2, the peak particle temperature achieves the lowest value, which is considered as the optimized design. The diameter of the particle increases, the heating power of a single particle increases also, and the average thermal conductivity of the pebble fuel remains the same, then the peak particle temperature increases monotonously. Therefore, an optimized

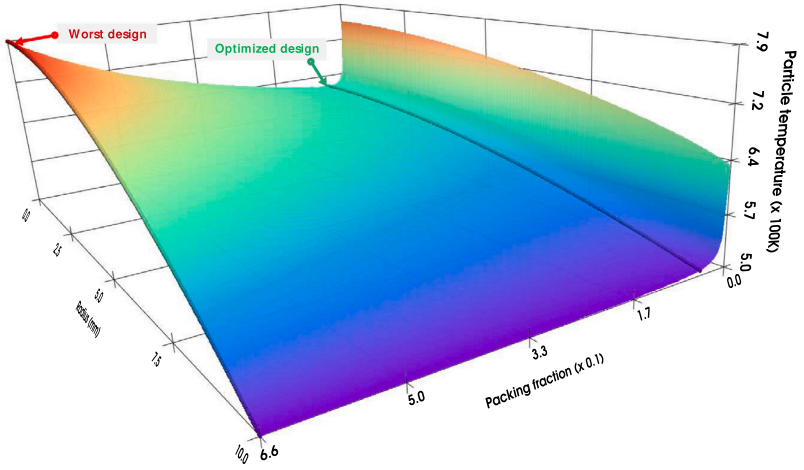

Fig. 10. Influence of packing fraction on the temperature distribution using ITM.

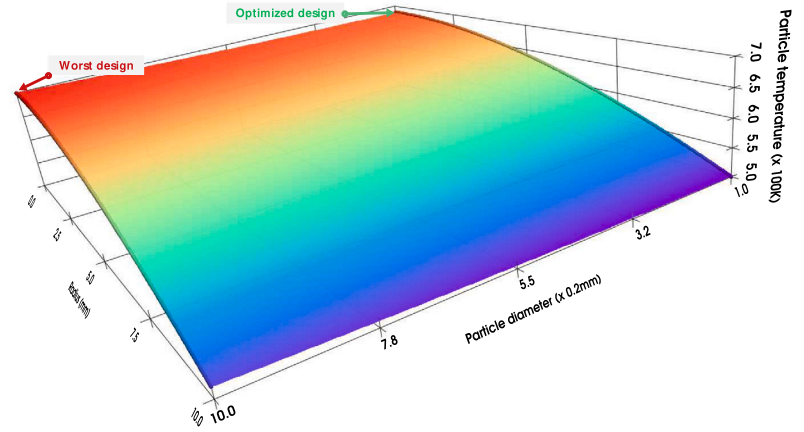

Fig. 11. Influence of particle diameter on the temperature distribution using ITM.

packing fraction and a smaller particle diameter should be adopted in the design of a TRISO pebble fuel.

In the present study, an improved two-temperature method (ITM) was developed, which capitalizes on the analogous nature of heat and neutron diffusion processes, both of which are based on the fundamental governing differential equation that the increasing heat in the control region equals the sum of the heat across all the surfaces of the region and the heat transferred from the region to the adjacent other material. ANSYS CFX software was used to calculate the heat transport in a pebble fuel, providing results for validation of the ITM. In general, ITM can provide very accurate predictions of the peak temperature of both the fuel particles and the matrix, and an optimized packing fraction and a smaller particle diameter should be adopted in the design of a TRISO pebble fuel, which were concluded from the analysis of the influences of packing fraction and particle diameter on the temperature distribution within a pebble fuel.

In theory, ITM can be applied to the pebble fuel with randomly packed particles. Future work could be investigating the influence of varying packing fraction along the radial direction within a pebble fuel, which is closer to the actual situations of a real TRISO-coated particle pebble fuel, especially at high burnup conditions.

6. Conclusions

In the present study, an improved two-temperature method (ITM) was developed, which capitalizes on the analogous nature of heat and neutron diffusion processes, both of which are based on the fundamental governing differential equation that the increasing heat in the control region equals the sum of the heat across all the surfaces of the region and the heat transferred from the region to the adjacent other material. ANSYS CFX software was used to calculate the heat transport in a pebble fuel, providing results for validation of the ITM. In general, ITM can provide very accurate predictions of the peak temperature of both the fuel particles and the matrix, and an optimized packing fraction and a smaller particle diameter should be adopted in the design of a TRISO pebble fuel, which were concluded from the analysis of the influences of packing fraction and particle diameter on the temperature distribution within a pebble fuel.

The main original works are in three aspects: (a) new equation structure of ITM in determining the temperature distributions within a TRISO-coated particle pebble fuel, as equation (1) describes; (b) new equations for determination of μ, A_f, and A_m, as shown in Eqs. (2)–(7); (c) new findings of the influences of the packing fraction. Main conclusions are summarized as below,

- Eq. (1) was proposed to calculate the temperature distributions within a TRISO-coated particle pebble fuel, for both the transients and steady state conditions, which are main equations of ITM.
- The determination of μ, A_f, and A_m were proposed and introduced in details, which are the key factors in the main equations of ITM.
- Seven tests were implemented for comparing ITM with finite element method, results show the ITM can provide very accurate

predictions of the peak temperature of both the fuel particles and the matrix, the predicting errors of all the cases are less than 1.2 K. Meanwhile, The temperature distributions within the pebble fuel are also well predicted by ITM.

- ITM was used to investigate the influences of packing fraction and particle diameter on the temperature distribution within a pebble fuel. Results show there are two competing mechanisms resulting in the optimized design occurs at the packing fraction of 0.05, and the smallest particle diameter of 0.2 mm.
- Future work could be investigating the influence of varying packing fraction within a pebble fuel, which is closer to the actual situations of a real TRISO-coated particle pebble fuel, especially at high burnup conditions.

Nomenclature

A_f	Ratio of the fuel particle diffusion surface area to the complete surface area, [−]
A_m	Ratio of the graphite matrix diffusion surface area to the complete surface area, [−]
F	Empirical coefficient relevant to the packing fraction of particles, [−]
d	Differential operator, [−]
k_e	Predicted effective thermal conductivity of the pebble fuel, [W/(m K)]
k_f	Thermal conductivity of fuel particle, [W/(m K)]
k_m	Thermal conductivity of graphite matrix, [W/(m K)]
k_s	Thermal conductivity of pebble shell, [W/(m K)]
M_f	Volumetric heat capacity of fuel particle, [J/(m^3 K)]
M_m	Volumetric heat capacity of graphite matrix, [J/(m^3 K)]
M_s	Volumetric heat capacity of pebble shell, [J/(m^3 K)]
n	Number of fuel particles, [−]
q	Homogenized volumetric heat generation rate, [W/m^3]
Q_μ	Heating power, [W]
r	Radius, [m]
r_f	Radius of the fuel particle, [m]
r_μ	Radius of the hypothetical calculation model for parameter μ, [m]
S	Scaling ratio of the arrangement of the particles, [−]
t	Time, [s]
T_f	Temperature of fuel particle, [K]
T_m	Temperature of graphite matrix, [K]
T_s	Temperature of pebble shell, [K]
V_μ	Volume of the hypothetical calculation model for parameter μ, [m^3]
V_p	Volume of the pebble fuel, [m^3]
V_f	Volume of the fuel particle, [m^3]
V_m	Volume of the matrix, [m^3]
Greek symbols	
μ	Region heat transfer coefficient, [W/(m^3 K)]
ϵ	Packing fraction of the particles, [−]
Abbreviations	
BCC	Body-centered cubic
HPR	Heat pipe reactor
IPyC	Inner pyrolytic carbon
OPyC	Outer pyrolytic carbon
SiC	Silicon carbide
TRISO	Tristructural-isotropic
ITM	Improved two-temperature method
VHTR	Very high-temperature reactor

CRediT authorship contribution statement

Dali Yu: Writing – review & editing, Writing – original draft, Validation, Methodology, Investigation, Funding acquisition, Formal analysis, Data curation, Conceptualization. **Fangnian Wang:** Methodology, Formal analysis. **Huaping Mei:** Funding acquisition, Data curation. **Xiongwei Cheng:** Software, Methodology. **Chengjun Duan:** Validation, Software.

Declaration of competing interest

The authors declare that they do not have any financial or nonfinancial conflict of interests.

Acknowledgments

This work was supported by the International Partnership Program of Chinese Academy of Sciences (145GJHZ2024054MI), National Natural Science Foundation of China (52306291), Anhui Provincial Natural Science Foundation (2308085MA21), and Anhui Provincial Key Research and Development Project (2022107020018). We like to thank the Institutional Center for Shared Technologies and Facilities of INEST, HFIPS, CAS for providing research facilities.

References

[1] J. Sun, Z.G. Li, C. Li, et al., Progress of establishing the China-Indonesia joint laboratory on HTGR, Nucl. Eng. Des. 397 (2022) 111959, http://dx.doi.org/10.1016/j.nucengdes.2022.111959.

[2] A. Koster, H.D. Matzner, D.R. Nicholsi, PBMR design for the future, Nucl. Eng. Des. 222 (2003) 231–245, http://dx.doi.org/10.1016/S0029-5493(03)00029-3.

[3] J.E. Kelly, Generation IV international forum: A decade of progress through international cooperation, Prog. Nucl. Energ. 77 (2014) 240–246, http://dx.doi.org/10.1016/j.pnucene.2014.02.010.

[4] X.Y. Cai, S.Z. Qiu, W.X. Tian, et al., Development of a thermal–hydraulic analysis code for the pebble bed water-cooled reactor, Nucl. Eng. Des. 241 (2011) 4978–4988, http://dx.doi.org/10.1016/j.nucengdes.2011.09.007.

[5] G.Z. Xu, Z.N. Sun, X.K. Meng, et al., Flow boiling heat transfer in volumetrically heated packed bed, Ann. Nucl. Energy 73 (2014) 330–338, http://dx.doi.org/10.1016/j.anucene.2014.06.038.

[6] X.W. Chen, Y. Dai, R. Yan, et al., Experimental study on the vibration behavior of the pebble bed in PB-FHR, Ann. Nucl. Energy 139 (2020) 107193, http://dx.doi.org/10.1016/j.anucene.2019.107193.

[7] D.L. Yu, M.J. Peng, Z.Y. Wang, CFD study on the supercritical carbon dioxide cooled pebble bed reactor, Nucl. Eng. Des. 281 (2015) 88–95, http://dx.doi.org/10.1016/j.nucengdes.2014.11.030.

[8] F.Y. Zhang, G.F. Zhu, Y. Zou, et al., Conceptual design and neutronic analysis of a megawatt-level vehicular microreactor based on TRISO fuel particles and S-CO_2 direct power generation, Nucl. Sci. Tech. 33 (2022) 69, http://dx.doi.org/10.1007/s41365-022-01064-4.

[9] F.Y. Zhang, G.F. Zhu, Y. Zou, et al., Core nuclear design and heat transfer analysis of a megawatt-level SiC coated particle based vehicular micro reactor, Nucl. Eng. Des. 415 (2023) 112668, http://dx.doi.org/10.1016/j.nucengdes.2023.112668.

[10] D. Price, N. Roskoff, M.I. Radaideh, et al., Thermal modeling of an eVinci™-like heat pipe microreactor using openfoam, Nucl. Eng. Des. 415 (2023) 112709, http://dx.doi.org/10.1016/j.nucengdes.2023.112709.

[11] X.Y. Guo, Y.C. Guo, S.M. Guo, et al., Concept design and neutronics analysis of a heat pipe cooled nuclear reactor with CERMET fuel, Ann. Nucl. Energy 192 (2023) 109974, http://dx.doi.org/10.1016/j.anucene.2023.109974.

[12] D.L. Yu, J. Liu, C.J. Hu, et al., Key features and highly effective prediction of complete startup from frozen state for high-temperature heat pipe in heat pipe reactor, Appl. Therm. Eng. 236 (2024) 121766, http://dx.doi.org/10.1016/j.applthermaleng.2023.121766.

[13] Y. Ji, Z.G. Li, J. Sun, et al., Numerical investigation and parametric study on thermal-hydraulic characteristics of particle bed reactors for nuclear thermal propulsion, Nucl. Technol. 206 (2020) 1155–1170, http://dx.doi.org/10.1080/00295450.2020.1760703.

[14] M.H. Rabir, A.F. Ismail, M.S. Yahya, A micro-sized high-temperature thorium reactor with duplex TRISO fuel with enhanced thorium utilization compared to the SBU configuration, Fuel 354 (2023) 129316, http://dx.doi.org/10.1016/j.fuel.2023.129316.

[15] G.W. Helmreich, D.R. Brown, B. Blamer, Evaluation of pebble scanning strategies for fuel qualification by simple simulated radiography, Nucl. Eng. Des. 383 (2021) 111418, http://dx.doi.org/10.1016/j.nucengdes.2021.111418.

[16] J. Li, J. Sun, D. She, et al., Influence of input data uncertainties on failure probability of TRISO-coated particle, Ann. Nucl. Energy 163 (2021) 108561, http://dx.doi.org/10.1016/j.anucene.2021.108561.
[17] P.V. Uffelen, Modelling of Nuclear Fuel Behaviour, Institute for Transuranium Elements at EU-JRC No. EUR-22321-EN, 2006.
[18] L. Zou, G.J. Hu, D. O'Grady, R. Hu, Explicit modeling of pebble temperature in the porous-media model for pebble-bed reactors, Prog. Nucl. Energy 146 (2022) 104175, http://dx.doi.org/10.1016/j.pnucene.2022.104175.
[19] Y.J. Wu, B.K. Liu, H. Zhang, J. Guo, F. Li, A multi-level nonlinear elimination-based JFNK method for multi-scale multi-physics coupling problem in pebble-bed HTR, Ann. Nucl. Energy 176 (2022) 109281, http://dx.doi.org/10.1016/j.anucene.2022.109281.
[20] H. Zhang, J. Guo, J. Lu, F. Li, et al., An assessment of coupling algorithms in HTR simulator TINTE, Nucl. Sci. Eng. 3 (2018) 287–309, http://dx.doi.org/10.1080/00295639.2018.1442061.
[21] J. Wang, An Integrated Performance Model for High Temperature Gas Cooled Reactor Coated Particle Fuel (Doctoral Theses), Massachusetts Institute of Technology, 2004.
[22] A. García-Berrocal, C. Montalvo, J. Blázquez, Temperature transients in TRISO type fuel, Ann. Nucl. Energy 76 (2015) 172–176, http://dx.doi.org/10.1016/j.anucene.2014.09.031.
[23] M. Grimod, R. Sanchez, F. Damian, A dynamic homogenization model for pebble bed reactors, J. Nucl. Sci. Technol. 52 (2015) 932–944, http://dx.doi.org/10.1080/00223131.2015.1037809.
[24] G.C.J. Bart, Thermal Conduction in Non Homogeneous and Phase Change Media (Doctoral Theses), Delft University of Technology, 1994.
[25] Y. Chiew, E. Glandt, The effect of structure on the conductivity of a dispersion, J. Colloid Interf. Sci. 94 (1983) 90–104, http://dx.doi.org/10.1016/0021-9797(83)90238-2.
[26] C. Folsom, C.H. Xing, C. Jensen, et al., Experimental measurement and numerical modeling of the effective thermal conductivity of TRISO fuel compacts, J. Nucl. Mater. 458 (2015) 198–205, http://dx.doi.org/10.1016/j.jnucmat.2014.12.042.
[27] M.L. Liu, J. Thurgood, Y.H. Lee, et al., Development of a two-regime heat conduction model for TRISO-based nuclear fuels, J. Nucl. Mater. 519 (2019) 255–264, http://dx.doi.org/10.1016/j.jnucmat.2019.04.004.
[28] C.X. Wu, G.T. Yang, W. Zhang, et al., Numerical study of TRISO particles with random size and location distribution in cuboid and cylindrical matrix: A validation for two-regime heat conduction model, Nucl. Eng. Des. 423 (2024) 113193, http://dx.doi.org/10.1016/j.nucengdes.2024.113193.
[29] M.K. Cai, T.L. Cong, H.Y. Gu, Multiphysics fuel performance modeling of dispersed TRISO-coated particle fuel plate under long-time normal condition and accident conditions, Nucl. Eng. Des. 415 (2023) 112725, http://dx.doi.org/10.1016/j.nucengdes.2023.112725.
[30] M.H. Wang, S.S. Bu, B. Zhou, et al., Multi-scale heat conduction models with improved equivalent thermal conductivity of TRISO fuel particles for FCM fuel, Nucl. Eng. Technol. 55 (2023) 1140–1151, http://dx.doi.org/10.1016/j.net.2022.12.001.
[31] M.H. Wang, S.S. Bu, B. Zhou, et al., Macroscopic transport characteristics in packed bed with a multi-physics inversion strategy for solid breeding blanket of HCCB TBM, Appl. Therm. Eng. 247 (2024) 123114, http://dx.doi.org/10.1016/j.applthermaleng.2024.123114.
[32] W. Jiang, J.D. Hales, B.W. Spencer, et al., TRISO particle fuel performance and failure analysis with BISON, J. Nucl. Mater. 548 (2021) 152795, http://dx.doi.org/10.1016/j.jnucmat.2021.152795.
[33] J.J. Gong, R.D. Yuan, X.Q. Song, et al., Numerical analysis of effective thermal conductivity of FCM with multilayer TRISO particle, Nucl. Mater. Energy 36 (2023) 101501, http://dx.doi.org/10.1016/j.nme.2023.101501.
[34] J.C. Wang, G.Q. Lu, M. Ding, Parametric study of effective thermal conductivity for VHTR fuel pebbles based on a neutronic and thermal coupling method, Ann. Nucl. Energy 181 (2023) 109530, http://dx.doi.org/10.1016/j.anucene.2022.109530.
[35] J.C. Wang, Z. Li, M. Ding, Study of the neutronic and thermal coupling effect on VHTR fuel pebble using openmc and openfoam, Ann. Nucl. Energy 183 (2023) 109643, http://dx.doi.org/10.1016/j.anucene.2022.109643.
[36] J. Shentu, S. Yun, N.Z. Cho, A Monte Carlo method for solving heat conduction problems with complicated geometry, Nucl. Eng. Technol. 39 (2007) 207–214, http://dx.doi.org/10.5516/NET.2007.39.3.207.
[37] N.Z. Cho, H. Yu, J.W. Kim, Two-temperature homogenized model for steady-state and transient thermal analyses of a pebble with distributed fuel particles, Ann. Nucl. Energy 36 (2009) 448–457, http://dx.doi.org/10.1016/j.anucene.2008.11.031.